Available online at www.scholarsresearchlibrary.com

Scholars Research Library

Der Pharmacia Lettre, 2017, 9 [12]: 23-45
[http://scholarsresearchlibrary.com/archive.html]

Scholars Research Library
ISSN 0975-5071
USA CODEN: DPLEB4

Experimental and Theoretical Approach Studies for 7- (1,3-Dioxolan-2-yl methyl)-3,7-Dihydro-1,3-Dimethyl-1h-Purine-2,6-Dione Using DFT

Suhasini M[1], Sailathaa E, Gunasekaran S[2], Ramkumaar GR[3]

[1]*Post Graduate and Research Department of Physics, Pachaiyappa's College, Chennai, TN, India*
[2]*Department of Research and Development, St. Peter's Institute of Higher Education and Research, St. Peter's University, Avadi, Chennai, TN, India*
[3]*Department of Physics, C. Kandaswami Naidu College for Men in Anna Nagar East, Chennai, TN, India*

***Corresponding author:** Suhasini M, Post Graduate and Research Department of Physics, Pachaiyappa's College, Chennai 600030, TN, India, Tel: +91 7299840500; E-mail: suhasinimallu@gmail.com*

ABSTRACT

A new generation xanthine based bronchodilator 7- (1,3-dioxolan-2-ylmethyl)-3,7-dihydro-1,3-dimethyl-1H-purine-2,6-dione (DYDP), anti-asthmatic drug was investigated by theoretical DFT studies and experimental UV-Vis, FT-IR and FT-Raman analyses. Quantum chemical calculation (DFT) results have been used to predict and interpret the experimental results. The geometric structure of title molecule, molecular electrostatic potential (MEP), thermodynamic parameters, HOMO and LUMO energies were determined. NLO behaviour of the title molecule has been investigated by the determination of the first order hyperpolarizability, polarizability, and the dipole moment. Mulliken charges and the global reactivity descriptors of the title compound were predicted. The theoretical 13C chemical shift results were also calculated using the gauge independent atomic orbital (GIAO) approach and are in good correlation with experimental results.

Keywords: *Scutellaria barbata* D, Wound healing, Excision wound, Burn wound

INTRODUCTION

7- (1,3-dioxolan-2-ylmethyl)-3,7-dihydro-1,3-dimethyl-1H-purine-2,6-dione (DYPD) is a new bronchodilator xanthine based drug. It is a purine alkaloid possessing pharmacological properties. It is used in the treatment of bronchial asthma, chronic obstructive pulmonary disease (COPD) [1] and chronic bronchitis. It has anti-tussive and bronchodilator effects and acts as a phosphodiesterase inhibitor. Also it is used as therapeutic agent anti-inflammatory activities [2] and a bronchodilating effect on smooth muscle [3]. It is structurally different from theophylline and a potential alternative to patients susceptible to harmful cardiac effects of bronchodilator therapies [4]. Unlike other bronchodilators, it is devoid of direct stimulatory adverse effects on cardiovascular, central nervous and gastrointestinal systems [5-7]. It is also used in the prevention of bronchial hyper reactivity induced by platelet-activating factors in animals [8]. In view of its favorable therapeutic effects, there is a great need for analytical methods to ensure the quality and safety of DYPD in bulk drugs and its formulations. It molecular formula is C11H14N4O4. The molecular mass of DYPD is 266.25 g/mol. The molecular structure of DYPD is shown Figure 1. The main aim of the present manuscript is to study the spectroscopic parameters of DYPD drug using FT-Raman,FT-IR and UV-Visible spectroscopic techniques and theoretical studies using Density Functional Theory (DFT).

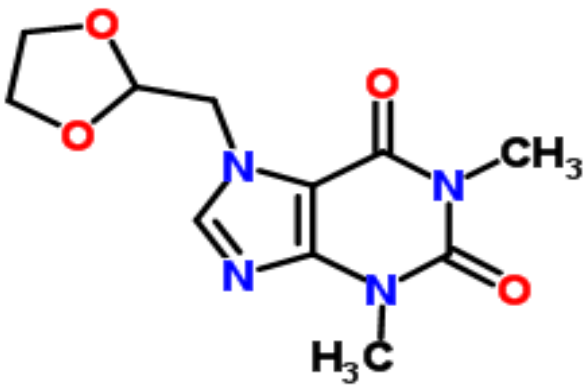

Figure 1: Molecular structure of DYPD.

MATERIALS AND METHODS

The sample of DYPD was procured in the solid form from a reputed pharmaceutical firm and used as received without further purification. The UV-Visible spectral measurements were recorded on Lambda 35 UV-VIS spectrometer. The Raman spectrum of title compound was recorded on Bruker IFS 66 V spectrometer using 1064 (nm) line of Nd:YAG laser in the wave length range 4000–50 cm^{-1}. The Bruker IFS 66 V spectrometer was used to record Fourier transform Infra-Red (FT-IR) spectrum of DYPD using KBr pellet method. FT-IR of the compound was recorded in the range of 4000-400 cm^{-1}.

Quantum chemical calculations

Density functional theory describes the physico-chemical properties accurately and presents a good balance between accuracy and computing economy. The all theoretical calculations were carried out on Gaussian 09 program [9] using DFT (B3LYP) method with 6-31G (d, p) basis set. 13C NMR chemical shift values of the title molecule were also calculated using the gauge

independent atomic orbital (GIAO) approach [10] by the same method. Using the same level of theory, the optimization of the molecular geometry, thermodynamic parameters, fundamental vibrational frequencies have been calculated. The harmonic vibrational frequencies calculated at B3LYP/6-31G (d, p) level and were compared against experimental values. Using Veda 4 program [11], calculations of the potential energy distribution (PED) were done. HOMO and LUMO were determined by using time dependent (TD) DFT method with B3LYP level. Mulliken charges, molecular electrostatic potential and the global reactivity descriptors of the title molecule were also calculated. Non-linear optical behaviour of the title compound has also investigated using the same level of theory.

RESULTS AND DISCUSSION

Structural analysis

The X-ray crystal structural analysis of DYPD was reported by Hai-Xiang Chen et al. [12]. In the present study, the molecular structure along with labeling of atoms of the DYPD (Figure 2) was obtained from the analysis carried out on Gaussian 09 software package. The reported experimental values and optimized structural parameters (bond lengths and bond angles) calculated by DFT (B3LYP) with 6-31G (d, p) basis set are summarized in Table 1. Marginal differences between the experimental and calculated values have been observed. The differences are due to the fact that the experimental values were for the molecule in the solid state associated with intermolecular interactions whereas the theoretical values were for a gaseous molecule. The bond length between C8–C9 is 1.433 Å in B3LYP method which is in reasonable agreement with the experimental value of 1.422 Å. The bond length between C4 and N5 in B3LYP/6-31G (d, p) is 1.377 Å which is in good agreement with experimental value of 1.373. The bond angle between C2-N1-C14 is 127.8 as estimated by B3LYP method and is in exact agreement with experimental value of 127.8°. The bond angle between N5-C4-C9 is 121.5° by B3LYP method which is in good agreement with experimental value of 121.6°.

Table 1: Optimized geometric parameters of DYPD molecule computed at DFT/B3LYP with 6-31G (d, p) basis set.

Parameters	B3LYP/6-31G (d, p)	Experimental Value
Bond length (A°)		
N1-C2	1.356	1.341
N1-C9	1.390	1.384
N1-C14	1.460	1.459
C2-N3	1.330	1.335
C2-H20	1.080	0.930
N3-C4	1.360	1.350
C4-N5	1.377	1.373
C4-C9	1.380	1.360

N5-C6	1.391	1.374
N5-C12	1.463	1.472
C6-N7	1.411	1.395
C6-O10	1.223	1.200
N7-C8	1.413	1.410
N7-C13	1.467	1.468
C8-C9	1.433	1.422
C8-O11	1.230	1.220
C12-H21	1.089	0.960
C12-H21	1.092	0.960
C12-H23	1.092	0.960
C13-H24	1.087	0.960
C13-H25	1.092	0.960
C13-H26	1.092	0.960
C14-C16	1.525	1.484
C14-H27	1.094	0.970
C14-H28	1.091	0.970
O15-C16	1.414	1.401
O15-C19	1.427	1.403
C16-O17	1.421	1.404
C16-H29	1.103	0.980
O17-C18	1.432	1.425
C18-C19	1.532	1.477
C18-H30	1.097	0.970
C18-H31	1.094	0.970
C19-H32	1.100	0.970
C19-H33	1.092	0.970
Bond angle (°)		
C2-N1-C9	105.7	105.4
C2-N1-C14	127.8	127.8
C9-N1-C14	126.5	126.6
N1-C2-N3	113.5	113.8
N1-C2-H20	121.4	123.1
N3-C2-H20	125.1	123.1
C2-N3-C4	103.8	103.1
N3-C4-N5	126.6	126.1
N3-C4-C9	111.8	112.3
N5-C4-C9	121.5	121.6
C4-N5-C6	120.2	119.8

C4-N5-C12	121.9	121.1
C6-N5-C12	118.0	119.1
N5-C6-N7	116.6	117.0
N5-C6-O10	121.0	121.7
N7-C6-O10	122.5	121.3
C6-N7-C8	126.9	126.8
C6-N7-C13	117.3	116.3
C8-N7-C13	115.7	117.0
N7-C8-C9	111.6	111.3
N7-C8-O11	121.2	121.4
C9-C8-O11	127.2	127.3
N1-C9-C4	105.1	105.4
N1-C9-C8	131.7	131.0
C4-C9-C8	123.2	123.6
N5-C12-H21	107.7	109.5
N5-C12-H22	110.1	109.5
N5-C12-H23	110.0	109.5
H21-C12-H22	110.3	109.5
H21-C12-H23	110.3	109.5
H22-C12-H23	108.4	109.5
N7-C13-H24	107.8	109.5
N7-C13-H25	109.8	109.5
N7-C13-H26	109.8	109.5
H25-C13-H26	110.7	109.5
N1-C14-C16	110.7	113.0
N1-C14-H27	108.2	109.0
N1-C14-H28	112.4	109.0
C16-C14-H27	110.0	109.0
C16-C14-H28	107.2	109.0
H27-C14-H8	108.5	107.8
C16-O5-C9	109.2	106.6
C14-C16-O15	109.5	111.4
C14-C16-O17	105.1	109.1
C14-C16-H29	110.7	109.6
O15-C16-O17	107.1	107.3
O15-C16-H29	110.3	109.6
O17-C16-H29	109.5	109.6
C16-O7-C18	108.3	108.2
O17-C18-C19	103.5	105.0

O17-C18-H30	109.8	110.7
O17-C18-H31	109.4	110.7
C19-C18-H30	111.8	110.7
C19-C18-CH31	113.2	110.7
H30-C18-H31	109.1	108.8
O15-C19-C18	102.2	105.5
O15-C19-H32	110.7	110.6
O15-C19-H33	108.5	110.6
C18-C19-H32	111.5	110.6
C18-C19-H33	114.3	110.6
H32-C19-H33	109.4	108.8

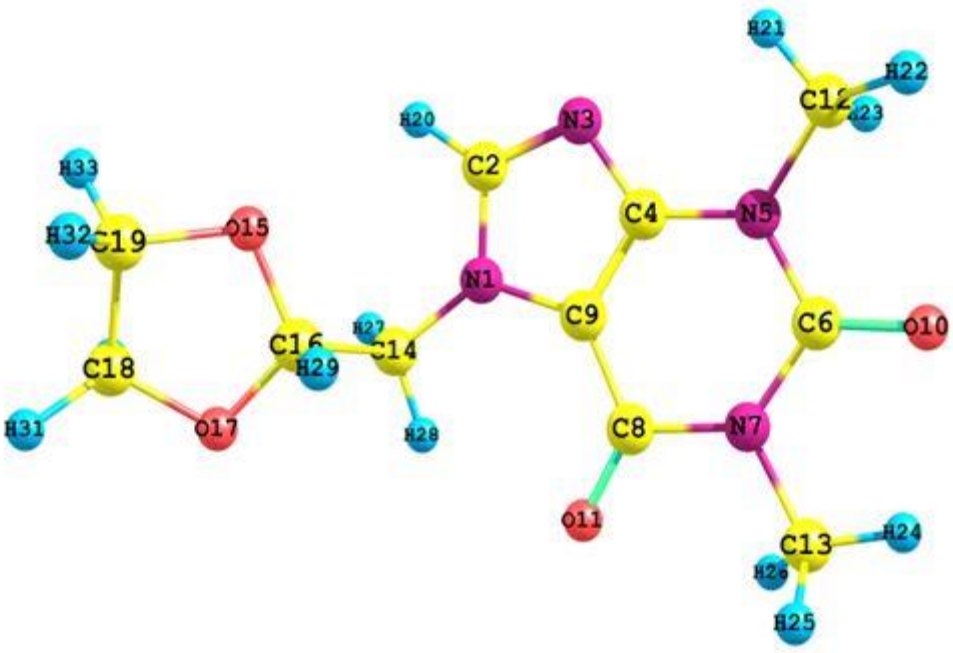

Figure 2: The optimized molecular structure of DYPD.

Frontier molecular orbitals

The frontier molecular orbitals (FMOs) called highest occupied molecular orbital (HOMO), and the lowest unoccupied molecular orbital (LUMO) are the most important orbitals in the molecule. The HOMO and LUMO play an important role in the optical and electronic properties of molecules [13,14]. Fully optimized ground-state structure has been used to determine energies of HOMO, LUMO at TD-DFT/B3LYP level of theory and the plots are shown in Figure 3. These are the main orbitals which are taking part in the chemical reaction. HOMO and LUMO energies are directly related to the ionization potential and electron affinity respectively. Also the frontier orbital gap (the energy gap between HOMO and LUMO), represents the stability of the structures

and helps to characterize some significant issues including the kinetic stability as well as chemical reactivity of the molecule [15]. When the frontier orbital gap is small then the molecule is said to be more polarizable and is generally associated with low kinetic stability as well as high chemical reactivity [16]. The energy separation between HOMO and LUMO was found to be 0.18697 eV.

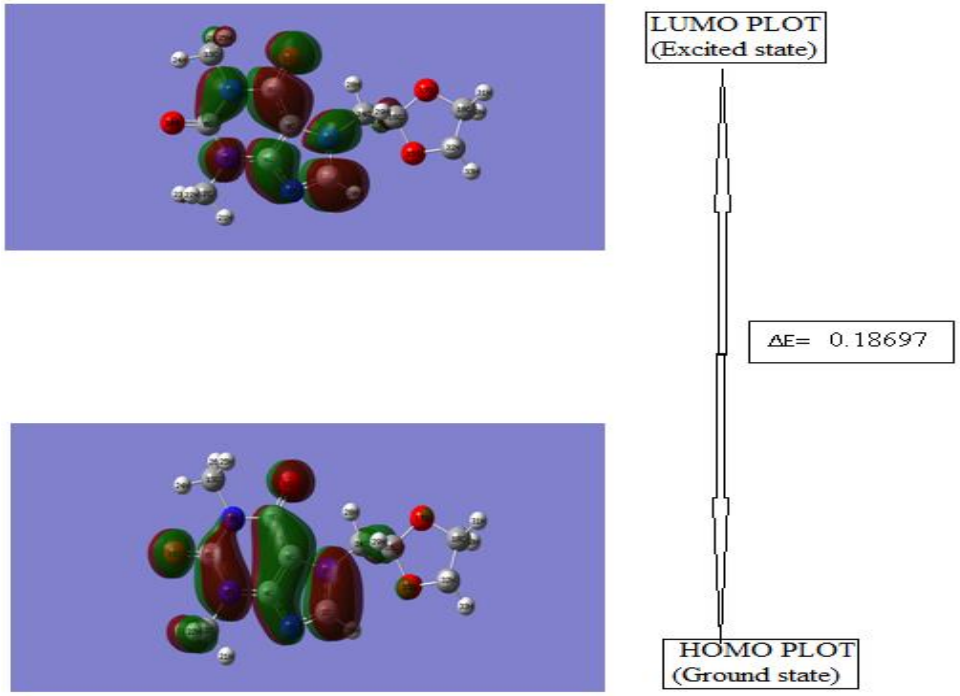

Figure 3: HOMO, LUMO orbitals at TD-DFT/B3LYP level of theory for DYPD.

UV-Vis studies

Theoretically, UV-Visible spectral data was calculated by TD-DFT method with B3LYP level and 6-31G (d, p) basis set. The calculations were made in gas phase. The UV-Vis absorption spectrum was recorded in DMSO (Dimethyl sulfoxide) and is shown in Figure 4. The experimentally observed and theoretically predicted wavelengths (λ_{max}) along with excitation energies (E, eV) and oscillator strength (f) are summarized in Table 2. In the experimentally recorded spectrum two prominent peaks were observed around 273 nm and 220 nm and were compared with the theoretically calculated wavelengths and found to be good agreement. The strong absorption band 273 nm caused by the n→π* and the other band 220 nm corresponds to π→π* assignment.

Table 2: Experimental and calculated wavelength (λ), excitation energies (E), and oscillator strengths (*f*) of DYPD using B3LYP/6-31G (d, p) level.

λ (Expt.; nm)	λ (Cal.; nm)	E (eV)	f
273	265.55	4.6690	0.1131
	251.30	4.9337	0.0001
220	219.07	5.6595	0.0387

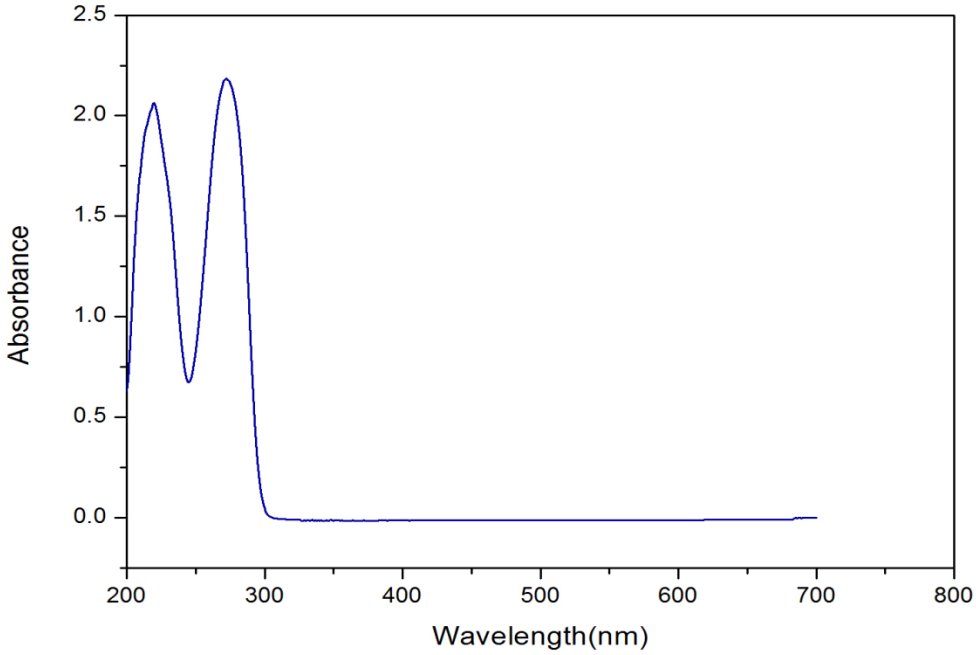

Figure 4: Experimental UV-Vis spectrum of DYPD.

Global reactivity descriptors

Softness (S), global hardness (η), electronegativity (χ) and electrophilicity index (ω) are commonly used as global reactivity parameters within density functional theory. In the present investigation, the energies of HOMO and LUMO, the frontier energy gap (ΔE), softness (S), electronegativity (χ) and electrophilicity index (ω) of the title molecule were calculated by B3LYP method with 6-31G (d, p) basis set and summarized in the Table 3.

According to Koopmans' theorem [17] the ionization potential (I) and electron affinity (A) can be expressed through HOMO and LUMO orbital energies:

I: Ionization potential ≈ - E_{HOMO}

A: Electron affinity ≈ - E_{LUMO}

ΔE_{gap}: the energy gap (eV) = E_{LUMO} - E_{HOMO}

χ: electronegativity = $\frac{(I+A)}{2}$

η: global hardness = $\frac{(I-A)}{2}$

S: softness = $\frac{1}{\eta}$

Parr et al. [18] have introduced global electrophilicity index (ω) which measures the propensity of a species to accept electrons.

ω: electrophilicity index = $\frac{\mu^2}{2\eta}$

where electrochemical potential =- electro negativity

$$\mu = -x$$

Table 3 Calculated global reactivity parameters of DYPD.

Basic sets	**Theoretical values**
E_{HOMO} (eV)	-0.21628
E_{LUMO} (eV)	-0.02931
$E_{HOMO-LUMO}$ gap (eV)	0.18697
Ionization potential (I)	0.21628
Electron affinity (A)	0.02931
global hardness (η)	0.093485
Softness (S)	5.34845
Chemical potential (μ)	-0.122795
Electronegativity (χ)	0.122795
Electrophilicity index (ω)	0.08065

Molecular electrostatic potential (MEP)

Molecular electrostatic potential is a powerful tool which provides insights into inter molecular association and molecular properties of small molecules, actions of drug molecules and their analogs [18]. MEP may be used to predict binding sites for electriphilic attack (electron rich region) and nucleophilic attack (electron poor region). The MEP surface simultaneously displays molecular size, shape and electrostatic potential in terms of colour coding and is a practical tool in the investigation of correlation between molecular structure and the physiochemical property relationship of molecules including bio molecules and drugs [19-24]. The red and blue region refers to the electron rich and electron poor region while green region in the MEP suggests almost the neutral potential. The variation in electrostatic potential produced by a molecule is largely responsible for the binding sites, as the binding site in general is expected to have opposite areas of electrostatic potential. The contour plot of the DYPD generated at optimized geometry of title molecule using Gauss view 05software is shown in Figure 5. For the molecule DYPD as can be seen Figure 5, electrophilic sites (negative region: red colour) are mainly over the oxygen atoms while the nucleophilic sites (positive region: blue colour) are around the nitrogen atoms.

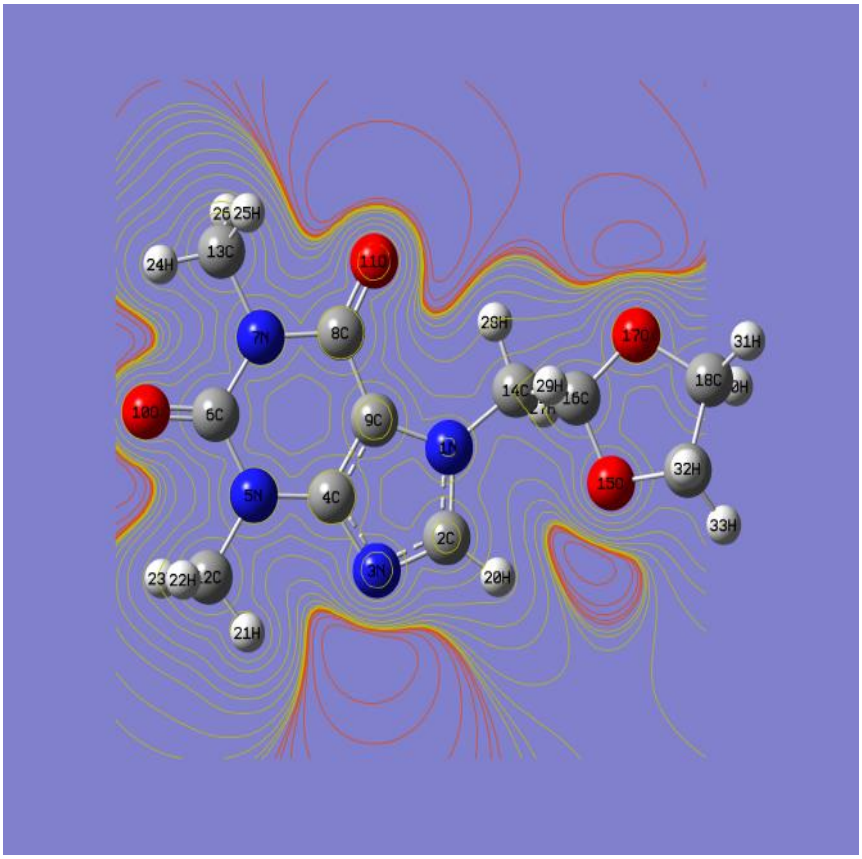

Figure 5: Electrostatic potential contour map of DYPD.

Thermodynamic properties

The standard thermodynamic functions such as heat capacity ($C^{\circ}_{p.m}$), entropy (S°_{m}), and enthalpy changes (ΔH°_{m}) for the title molecule were calculated on the basis of vibrational analysis and statistical thermodynamics and are listed in Table 4. The values of heat capacity, entropy and enthalpy all increased with the rise in temperature [25] from 100 to 1000 K as observed from Table 4. The correlation equations between heat capacity, entropy and enthalpy changes and temperatures are fitted by quadratic formulas and the corresponding fitting factors (R^2) for these thermodynamic properties were 0.99983, 0.99043 and 0.99956 for heat capacity, entropy and enthalpy respectively. The corresponding fitting equations are as follows and the correlation graph is shown in Figure 6.

$$C^{\circ}_{p.m} = 277.98134 + 1.09319\ T - 2.54325 \times 10^{-4}\ T^2 \qquad (R^2 = 0.99983)$$

$$S^{\circ}m = -56.15568 + 1.24319\ T - 5.85759 \times 10^{-4}\ T^2 \qquad (R^2 = 0.99043)$$

$$\Delta H^{\circ}_{m} = -9.38261 + 0.11772\ T + 2.78037 \times 10^{-4}\ T^2 \qquad (R^2 = 0.99956)$$

Table 4: Variation of thermodynamic properties with temperatures at B3LYP/6-31G (d, p) level for DYPD.

Temperature (K)	**$S^{\circ}m$ (cal mol^{-1} K^{-1})**	**$C^{\circ}_{p.m}$ (cal mo^{-1} K^{-1})**	**ΔH°_{m} (K cal mol^{-1})**
100	379.02	30.10	8.52
200	490.88	199.95	25.05
298.15	583.95	272.06	48.6
300	585.64	273.46	48.67
400	674.66	348.35	79.79
500	759.78	415.29	118.06
600	840.61	471.26	162.48
700	916.83	517.27	211.98
800	988.45	555.24	265.67
900	1055.73	586.85	322.82
1000	1118.98	613.39	382.87

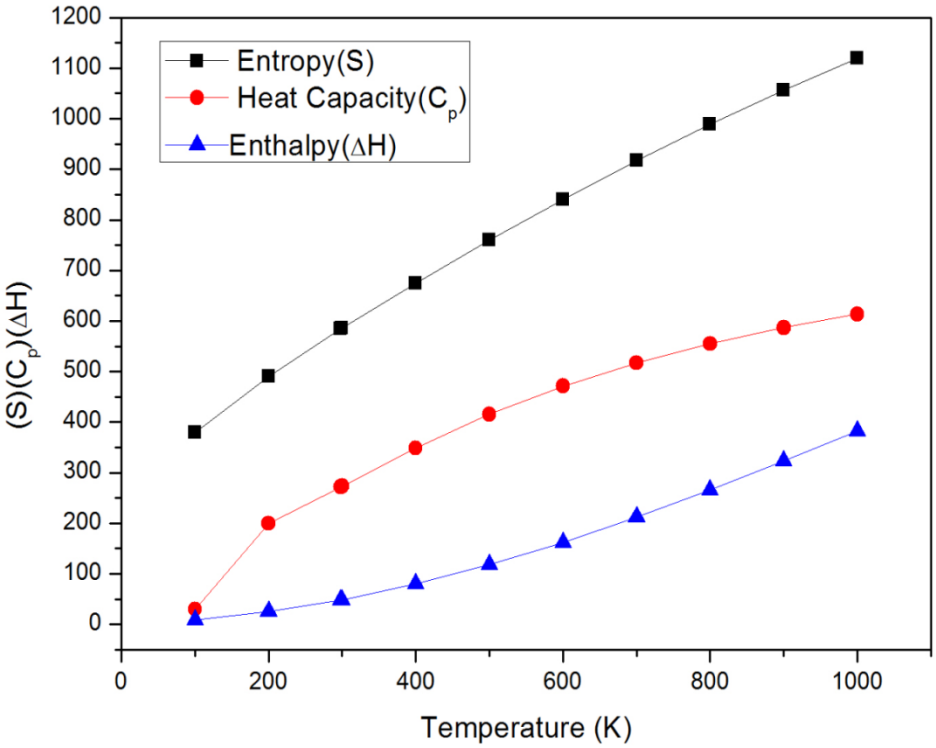

Figure 6: Correlation graph between thermodynamic parameters and temperature.

Mulliken atomic charges

The Mulliken charge is directly related to the vibrational properties of the molecule, and quantifies how the electronic structure changes under atomic displacement; it is therefore related directly to the chemical bonds present in the molecule. It affects dipole moment, polarizability, electronic structure and more properties of molecular systems. Mulliken population analysis (MPA) provides a partition of either a total charge density or an orbital density. The Mulliken atomic charges obtained by the B3LYP method with 6-31G (d, p) basis set for DYPD are given in Table 5. The magnitude of the carbon atomic charges is found to be positive and negative. All the hydrogen atoms have positive Mulliken charges. The atom C6 has the highest Mulliken charge (0.783) when compared to the other atoms. From the listed atomic charge values, the nitrogen (N5) atom had a large negative charge (-0.601 for B3LYP) and behaved as electron behaved as electron acceptor. The corresponding Mulliken's plot is shown in Figure 7.

Table 5: Mulliken population Analysis of DYPD by B3LYP/6-31G (d, p)

Numbered Atoms	B3LYP/6-31G (d, p)
N1	-0.534
C2	0.295

N3	-0.526
C4	0.473
N5	-0.601
C6	0.783
N7	-0.59
C8	0.645
C9	0.216
O10	-0.528
O11	-0.543
C12	-0.177
C13	-0.172
C14	-0.091
O15	-0.506
C16	0.427
O17	-0.515
C18	0.055
C19	0.019
H20	0.143
H21	0.151
H22	0.14
H23	0.141
H24	0.155
H25	0.135
H26	0.36
H27	0.132
H28	0.183
H29	0.096
H30	0.111
H31	0.113
H32	0.11
H33	0.122

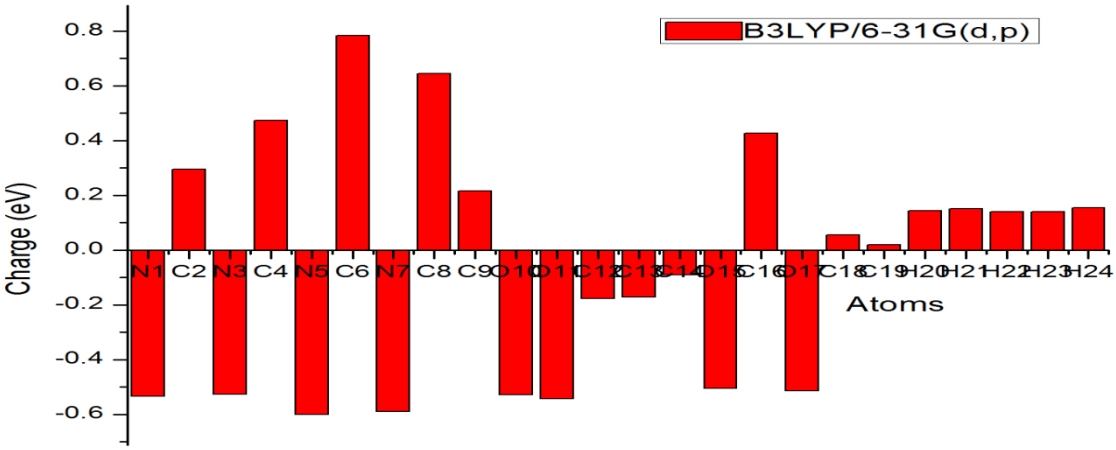

Figure 7: Mulliken atomic charges of DYPD

^{13}C Nuclear magnetic resonance (NMR) studies

Carbon nuclear magnetic resonance (^{13}C NMR) isotopic chemical shifts of DYPD drug were calculated using molecular structure at DFT-B3LYP/6-31G (d, p) level and Gauge Independent Atomic Orbital (GIAO) method (each atomic orbital has additional exponential term containing the vector potential) and are presented in Table 6 along with the experimental values [26]. In general, aromatic carbon resonances occur between 100-150 ppm [27,28]. However, with the attachment of more than one electron with drawing and electron donating substituents, the full range of aromatic resonances expand to 90–180 ppm. In the present work, from the calculated ^{13}C NMR spectrum, the carbon atom C8 appearing at very higher chemical shift value (157.17ppm in B3LYP/6-31G (d, p)) due to double bond of oxygen atom and Similarly C6, C4, and C2 appearing at higher chemical shift values (152.23, 151.10, and 143.72 ppm in B3LYP/6-31G (d, p)) are due to oxygen and nitrogen atoms O10, N5 and N3 respectively. The carbon atom C9 also appearing at higher chemical shift value (100.31 ppm in B3LYP/6-31G (d, p)) duo to nitrogen atom N1. The carbon atom C16 is highly electropositive and possess more positive charge than the other carbon atoms, and hence, the shielding is very small and appears up field (Table 6). In DFT calculated atomic charges revealed that the more electron-rich atoms are C12, C13, C14, C18 and C19 they are highly shielded atoms and appear at downfield (lower chemical shift). As observed from Table 6, the results obtained by using DFT (B3LYP) method are in reasonable agreement with experimental values. The results are close to experimental data and they differ slightly from results of experiment. As can be seen in Figure 8, there is a good linear relationship between experimental and theoretical B3LYP/6-31G (d, p) chemical shifts.

Table 6: Experimental and calculated ^{13}C NMR chemical shift values of DYPD.

Atoms	**Calculated by B3LYP/6-31G (d, p)**	**Experimental values**
C2	143.72	142.16
C4	151.10	148.22
C6	152.23	151.59
C8	157.17	155.25
C9	112.75	107.26
C12	38.39	29.69
C13	36.89	27.88

C14	56.94	47.87
C16	110.92	100.76
C18	73.65	65.37
C19	74.77	-

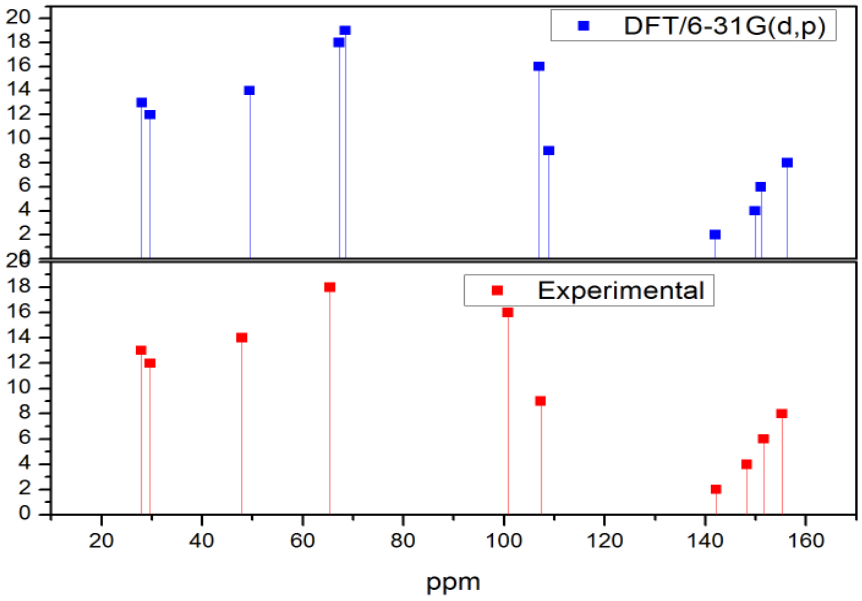

Figure 8: Calculated and Experimental ^{13}C NMR spectrum of DYPD

NLO analysis

Nonlinear optical (NLO) effects arises from the interactions of electromagnetic fields in various media to produce new fields altered in amplitude, frequency, phase or other propagation characteristics from the incident fields [29]. NLO is at the forefront of current research because of its importance in providing the key functions of optical switching, frequency shifting, optical logic, optical modulation and optical memory for emerging technologies in the areas such as signal processing, telecommunications and optical interconnections [30-33]. In the present work, NLO behaviour of DYPD was investigated by the determination of the polarizability (α), first order hyperpolarizability (β) and electric dipole moment (μ) by using the B3LYP method with 6-31G (d, p) basis set. Urea is the one of the prototypical molecules used in the comparing NLO properties of molecular systems. The calculated values of polarizability, first order hyperpolarizability and dipole moment for the title molecule were found to be

2.5340 × 10^{-23} e.s.u, 2.8203 × 10^{-30} e.s.u and 2.8635 D respectively at B3LYP/6-31G (d, p) level. The large β value (almost 7.6 times greater than urea) that indicates, the title compound is a good candidate of NLO material.

Vibrational analysis

DYPD has 33 atoms and optimized molecular geometry shows no special symmetries and consequently all the 93 (3N-6) fundamental vibrations of the title molecule are both IR and Raman active and are dispersed over the functional and fingerprint regions. The experimental and computed vibrational wave numbers, their IR intensities and detailed description of normal modes of vibration of DYPD carried out in terms of their contribution to the potential energy are given in Table 7. The experimental and the simulated infrared (IR) and the FT-Raman spectra of the title compound are shown in Figures 9 and 10.

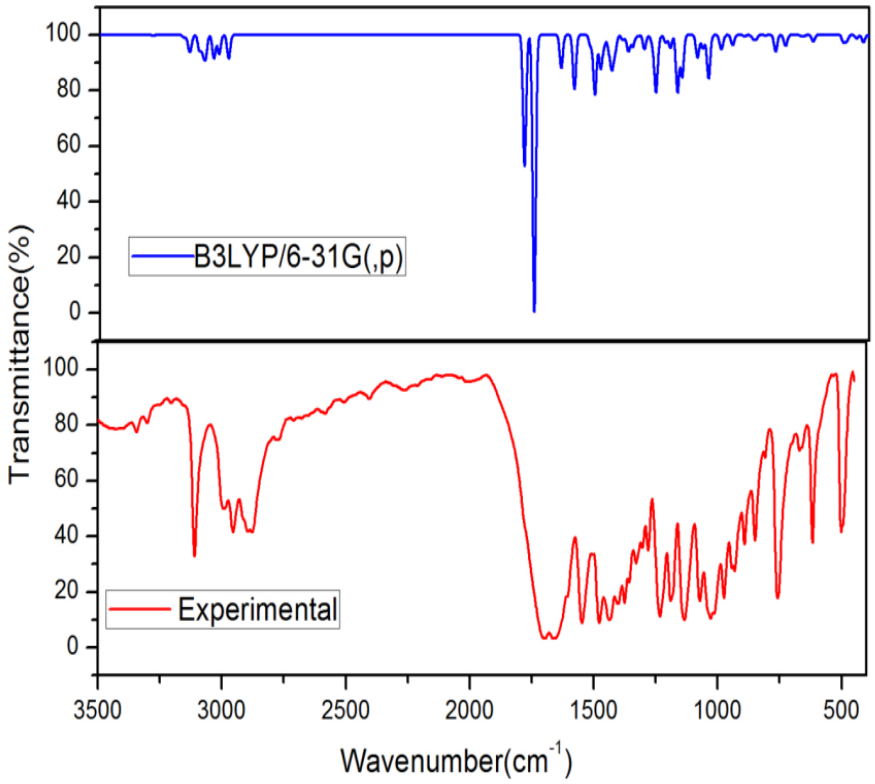

Figure 9: Experimental and calculated FT-IR spectrum of DYPD.

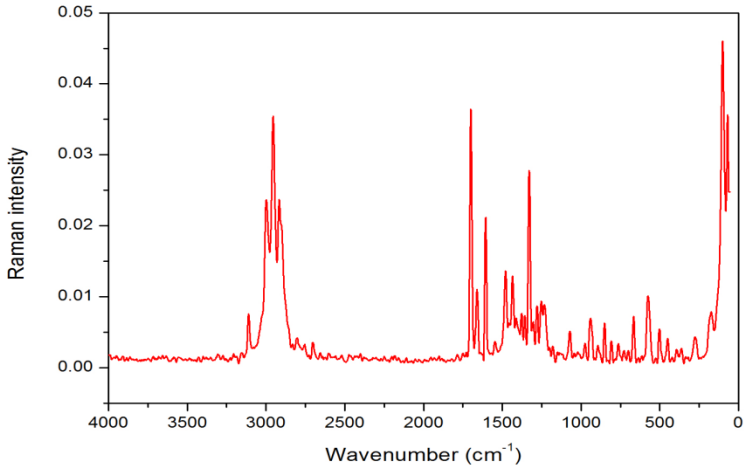

Figure 10: Experimental FT-Raman spectrum of DYPD.

C-H vibrations

Aromatic compounds commonly exhibit multiple weak bands in the region 3250-2950 cm^{-1} due to aromatic C-H stretching vibrations [34]. In the present study, FTIR bands observed at 3300 cm^{-1}, 3203 cm^{-1}, 3100 and 2990 cm^{-1} and the Raman bands 3110 cm^{-1} and 2998 cm^{-1} are due to C-H stretching vibrations. The C-H vibrations observed experimentally are in good agreement with the theoretically attained by DFT method.

C–C vibrations

The carbon–carbon stretching modes of the pyridine are expected in the range from 1650 to 1100 cm^{-1} [35]. Based on this in the present investigation, the experimental absorption band observed at 1660 cm^{-1} in the FTIR spectrum of pyridine and Raman bands observed at 1661, 1605 cm^{-1} are assigned as carbon-carbon stretching vibrations of the ring. These experimental carbon-carbon stretching vibrational bands are in reasonable agreement with the theoretically calculated ones.

C=N vibrations

The C=N and C–N stretching wave number in the side chains is a difficult task, because there are problems in identifying these wave numbers from other vibrations. In this work, the bands observed at 1477, 1438 and 1401 cm^{-1} in FT-IR spectrum and the bands observed at 1479 and 1435 cm^{-1} in FT-Raman spectrum are assigned to the C=N stretching vibrations [36], which are in good agreement with the calculated values.

C-O Vibrations

The C-O stretching vibrations in phenols are expected to appear as a strongest band in the 1260-1000 cm^{-1} frequency range [37]. In the present study, the bands observed at 1189,1071,1028 and 974 cm^{-1} in FT-IR spectrum and the bands obtained at 1179, 1070 and 974 cm^{-1} in FT-Raman spectrum is assigned as C-O stretching vibration. The C-O stretching vibration, with B3LYP/6-31G (d, p) predicated frequency of 1172,1070,1054,1046 and 992 cm^{-1} (Table 7).

C–C–N vibrations

In the present case, the C–C–N vibrations corresponds to 450 cm^{-1} in DFT method which are in good agreement with the experimental values Literature reference number [38] reports C–C–N in plane bending and out of plane bending vibrations at 428 and 160 cm^{-1} respectively. It is also supported by references [39,40].

Table 7: Experimental and calculated frequencies of DYPD using B3LYP/6-31G (d, p) method.

Experimental Wavenumber (cm^{-1})		**Calculated by B3LYP/6-31G (d, p)**		
FTIR	**FT-Raman**	**Frequency**	**Intensity**	**Assignments[a]**
3300		3287	1.9	νCH (99)
3203		3208	0.6	νCH (86)
		3189	0.6	νCH (92)
		3162	7.6	νCH (99)
		3142	19.3	νCH (97)
		3141	8	νCH (97)
		3135	24.6	νCH (92)
3100	3110	3100	38.6	νCH (97)
		3087	34.6	νCH (99)
		3077	25.1	νCH (100)
		3074	36.1	νCH (99)
		3041	62.1	νCH (97)
		3020	50.4	νCH (92)
2990	2998	2982	61.7	νCH (99)
		1788	345.0	νCH (72)
1698		1749	728.9	νCH (70)
1660	1661	1640	86.8	νCC (48)+νNC (25)
	1605	1587	143.1	βCCN (27)

1547	1546	1543	0.4	βHCH (81)
		1526	2	βHCH (79)
		1517	4.9	βHCH (63)+τHCNC (22)
		1508	8.1	τHCNC (13)
1504		1504	143.3	βHCH (37)
		1500	7.2	βHCH (76)+τHCNC (16)
1477	1479	1482	86.1	νNC (10)+βHCN (12)+βHCH (26)
		1468	26.7	βHCH (53)
		1545	10.8	τHCOC (21)
1438	1435	1436	79.8	νNC (12)+βHCN (13)+τHCOC (16)
		1424	41.8	τNC (23)
1401		1397	4.4	νNC (10)+βHCO (17)+τHCOC (12)
		1390	10.8	βHCO (28)+τHCOC (42)
1375	1377	1370	43.3	νNC (25)
1357	1357	1352	30.9	τHCNC (15)+τHCOC (14)
1328	1329	1332	4.8	βHCO (60)
1303		1305	36.7	νNC (29)+βCNC (20)
1280		1285	3.1	νNC (24)+βHCH (13)+τHCNC (34)
	1279	1272	22.3	βHCN (23)+βHCO (11)
		1259	140.4	νNC (11)+βHCN (30)
	1251	1251	19.8	βHCO (33)+τHCOC (19)
1232	1232	1229	1.5	βHCO (60)+τHCOC (35)
		1219	20.1	νNC (11)+βHCN (24)
		1200	33.1	βNCN (13)
1189	1179	1172	150.7	νOC (10)
		7761	0.1	τHCNH (40)
		1159	0.4	βHCH (24)+τHCNH (64)
1134		1153	109	νOC (10)+βHCO (17)+τCOCC (10)
		1097	3.3	νNC (12)
		1091	57.6	νCC (17)+νOC (12)+ΦOCOC (11)
1071	1070	1070	34.3	νOC (48)
		1054	13	νOC (30)
1028		1046	107.2	νNC (23)+ νOC (13)
1014		998	21.2	νNC (44)+βCNC (10)
974	974	992	20.1	νOC (54)
		953	4.2	βCOC (20)
942	939	949	23.4	νNC (11)+βCNC (12)

891	893	901	3.6	βCOC (28)+τHCOC (74)
		868	9.3	νOC (38)+νCC (14)+νHCNC (12)
849	850	856	10.9	τHCNC (84)+τCNCN (11)
808	808	818	1.6	βOCN (15)+βCCN (13)
	763	776	43.3	νNC (18)+βNCN (14)+βOCN (16)+ βOCC (10)
758		743	3.7	ΦONCC (17)+ΦONNC (64)
		737	0.1	νOC (16)+βOCO (43)
		736	26.7	τCCNC (20)+ΦONCC (26)+ ΦONNC (22)+ΦNCNC (11)
	700	701	0.3	τCCNC (17)+ΦNCNC (20)
		674	2.5	βCNC (13)+βCOC (11)
669	666	662	3.3	βCOC (37)
617		625	16.8	τCNCN (60)
533	576	571	0.3	νNC (39)
501	502	503	19.1	βNCN (27)
		490	15.9	βOCC (16)+βHCNC (15)+ ΦOCOC (20)
	450	450	8.9	νNC (20)+βNCN (10)+βCNC (21)
		422	18.8	βOCN (43)+βCNC (11)
		390	13.4	βOCC (19)+βNCN (13)+βCNC (19)
	363	370	9.2	βOCC (22)+βCNC (18)
		351	5.2	βCNC (32)+τCCN (12)+ΦNCNC (11)
		310	4.7	βCNC (57)
	276	276	0.2	ΦCCCN (55)
		273	1.9	νNC (11)+βCNC (21)+ΦOCOC (16)
		269	3.7	βCCN (10)+ΦCCCN (11)
		225	6.7	βCOC (10)+τHCOC (12)+τCOCC (38)
	173	184	6.5	βNCN (13)+βCNC (20)+ΦCCCN (10)
		156	4.6	τCNCC (28)+τNCNC (10)+τCNCN (18)
		140	2.3	ΦCCCN (50)+ΦNCNC (10)
		118	2.7	τNCNC (10)+τCNCN (44)
	101	98	0.3	τCNCC (13)+τNCNC (45)
		84	0.0	τHCNC (68)+ΦCCCN (10)
	69	61	2.2	τOCCN (30)+τCOCC (32)
		53	0.6	τOCCN (20)+ΦCCCN (32)
		47	0.7	τHCNC (67)
		42	1.5	τOCCN (30)+τCOCC (29)+ΦCCN (2)

		20	0.3	τCCNC (71)
Note: N - Stretching; B - Bending; τ- Torsion; ϕ - Out of Plane Bending, S - Scissoring, μ - Twisting, Ω - Wagging. A -Potential Energy Distribution (PED).				

CONCLUSION

The title compound was theoretically optimized using B3LYP with 6-31G (d, p) basis set. Thus, a complete vibrational band assignment of DYPD has been carried out using FTIR and FT-Raman spectra on the basis of their relative intensity, characteristic positions, correlation and vibrational bands of the related compounds. The good correlation is found between the computed and experimental wave numbers. NLO behaviour of the title molecule has been investigated by the dipole moment, polarizability and the first order hyperpolarizability. The electronic properties are also computed and compared with the experimental UV-Vis spectrum. The global reactivity descriptors like chemical potential, hardness, softness, electronegativity and electrophilicity index were calculated using density functional theory. Theoretical ^{13}C chemical shift values were reported and compared with experimental data, showing a very good agreement. Thermodynamic functions, MEP and Mulliken charges were also calculated using B3LYP method with 6-31G (d, p) basis set.

Acknowledgement

One of the authors Mrs. M. Suhasini is thankful to SAIF, IIT, Madras, for providing structural analysis of the title compound. My Sincere thanks to all the other authors for their support in all aspects.

REFERENCES

1. Nkar, J., Lodha, R., and Kabra, S.K., Doxofylline: The next generation methylxanthine, *Indian J. Pediatr*, **2008.** 75: 251-254.
2. Zhao, J.J., and Li, L., Doxofyllinium tetrachlorido-antimonate (III) monohydrate, *Acta Cryst*, **2001.** 27: 646-676.
3. Franzone, J.S., Reboani, C., and Fonzo, D., 7- (1,3-Dioxolan-2-ylmethyl)-1,3-di-methylpurine-2,6 (1H,3H)-dione trichloroacetic acid solvate, *Farmacol. Sci*, **1981.** 36: 201-219.
4. Dini, F.L., and Cogo, R., Doxofylline: A new generation xanthine bronchodilator devoid of major cardiovascular adverse effects, *Cur. Med. Res. Opin.* **2001.** 16: 258-268.
5. Daly, J.W., Bruns, R.F., and Snyder, S.H., Adenosine receptors in the central nervous system: relationship to the control action of methylxanthines, *Life Sci.* **1981.** 28: 2083-2097.
6. Fredholm, B.B., On the mechanism of action of theophylline and caffeine, *Acta Med. Scand.* **1985.** 217: 149-153.

7. Spealman, R.D., Psychomotor stimulant effects of methylxanthines in squirrel monkeys: relation to adenosine antagonism, *Psych. Pharm*. **1988.** 95: 19-25.
8. Franzone, J.S., Cirillo, R., and Biffignandi, P., Effect of doxofylline on PAF-induced bronchial hyper reactivity in guinea pigs, *Eur. J. Pharm*, **1989.** 165: 269-277.
9. Frisch, M.J., et al. *Gaussian, Inc*, Wallingford CT, **2009.**
10. Wolinski, K., Hinton, J.F, and Pulay, P., Efficient implementation of the gauge-independent atomic orbital method for NMR chemical shift calculations, *Journal of the American Chemical Society*, **1990.** 112: 8251-8260.
11. Jamroz, M.H., Vibrational energy distribution analysis VEDA 4 Program, Warsaw, **2004.**
12. Hai-Xiang, C. 7- (1,3-Dioxolan-2-ylmethyl)-1,3-dimethyl-3,7-dihydro-1H-purine-2,6-dione, *Acta Cryst*. **2007**. 63: 726–727.
13. www.sciencedirect.com/science/article/pii/S1386142515300330
14. Baranska, M., Kaczor, A., and Raman, J., Morphine studied by vibrational spectroscopy and DFT calculations. *Spectrosc.* **2012.** 43: 102-107.
15. Ebrahimi, H., Hadi, J.S., Amd Al-Ansari, H.S., *Journal of Molecular Structure*, **2013.** 1039: 37-45.
16. Fleming, I., Frontier orbitals and organic chemical reactions, *John Wiley & Sons, NY, USA*, **1976**.
17. Koopmans, T., Physica**. 1934**. 104-113.
18. Parr, RG, Szentpaly, L., and Liu, S.J., *Am. Chem. Soc.* **1999.** 121: 1922-1924.
19. Murray, J.S., and Sen, K, Concepts and applications, Elsevier, Amsterdam, **1996.**
20. Ggadre, S.R., and Shrivastava, I.H., and *J. Chem. Phys.* **1991.** 94: 4384-4390.
21. Alkorta, I., and Perez, J.J., *Int. J. Quant. Chem*. **1996.** 57: 123-135.
22. Scrocco, E., and Tomasi, J., Advances in quantum chemistry. 2, P. Lowdin, ed., Academic Press, New York, USA, **1978.**
23. Luque, F.J., SCRF calculation of the effect of water on the topology of the molecular electrostatic potential. *J. Phys. Chem.* **1993.** 97: 9380-9384.
24. Sponer, J., and Hobza, P., DNA base amino groups and their role in molecular interactions: *Ab initio* and preliminary density functional theory calculations. *Int. J. Quant. Chem.* **1996.** 57: 959-970.
25. Sajan, D., et al. *Spectrochim. Acta A*, **2011.** 81: 85-98.
26. https://newdrugapprovals.org/2013/12/04/drugspotlightdoxofylline/
27. Kalinowski, H.O., Berger, S., and Braun, S., Carbon-13 NMR spectroscopy, *John Wiley & Sons*, Chichester, **1988.**

28. Pihlaja, K., Kleinpeter, E., Carbon-13 chemical shifts in structural and stereochemical analysis. VCH Publishers, Deerfield Beach, **1994.**
29. Sun, Y.X., Graphene oxide doped polyaniline for supercapacitors. *J. Mol. Struct*. *Theochem*, **2009.** 904: 74–82.
30. Andraud, C., Solvent effects on nonlinear optical properties of novel para-nitroaniline derivatives: A density functional approach. *J. Am. Chem. Soc*., **1994.** 116: 2094-2102.
31. Geskin, V.M., Lambert, C., and Bredas, J.L., Origin of high second- and third-order nonlinear optical response in ammonio/borato diphenylpolyene zwitterions: The remarkable role of polarized aromatic groups. *J. Am. Chem. Soc*., **2003.** 125: 15651-15658.
32. Nakano, M., Theoretical study on second hyperpolarizabilities of phenylacetylene dendrimer: Toward an understanding of structure−Property relation in NLO responses of fractal antenna dendrimers. *J. Am. Chem. Soc*, **2002.** 124: 9648- 9655.
33. Sajan, D., Structural and electronic contributions to hyperpolarizability in methyl p-hydroxy benzoate. *J. Mol. Struct*, **2006.** 785: 43-53.
34. Socrates, G., Infrared characteristic group of frequencies. John Wiley & Sons, New York, USA. **1980.**
35. Sundaraganesan, N., et al. FT-IR, FT-Raman spectra and quantum chemical calculations of some chloro substituted phenoxy acetic acids. *Spectrochim. Acta A*, **2007.** 67: 214-224.
36. Silverstein, RM., Clayton Basseler, G., and Morill, C., Spectrometric identification of organic compounds. Wiley: New York, USA. **1981.**
37. Krishna Kumar V., and Prabavathi N., *Spectrochim. Acta A*, **2009.** 72: 738-742.
38. Sundaraganesan, N., FT-IR, FT-Raman spectra and quantum chemical calculations of 3,4-dimethoxyaniline, *Spectrochim. Acta A*, **2008.** 71: 1134-1139.
39. Prystupa, D.A., Anderson, A., and Torrie, B.H., Raman and infrared study of solid benzyl alcohol. J. *Raman Spectrosc.* **1994.** 25: 175.
40. Palafox, M.A., *Int. J. Quantum Chem*. **2000**. 77: 661.